Dependence of decaying homogeneous isotropic turbulence on inflow conditions

P. C. Valente and J.C. Vassilicos**

Department of Aeronautics, Imperial College London, London SW7 2AZ, United Kingdom

Abstract

A careful data analysis of far downstream turbulent flows generated by conventional and multiscale grids shows that these decaying flows are very clearly different from both Saffman and Loitsyansky turbulence. The analysis also shows that there are marked differences between the far downstream turbulence behaviors generated by different types of grid. There is an inflow condition dependence on both the normalised energy dissipation and the conserved large-scale invariant.

Keywords:

1. Introduction

A few years ago, Lavoie, Djenidi, and Antonia (2007) investigated potential effects of inflow conditions on the decay of approximately homogeneous isotropic turbulence. Inflow conditions refer to the way the turbulence is generated. In the wind tunnel experiments of these authors, the turbulence was passively generated by square-mesh biplane grids placed at the test section entry. A particular aspect of the potential dependence on inflow conditions is whether the power-law decay of the far-downstream turbulence depends on them. Quantitatively, the question is whether the decay exponent n in

$$u^2 \sim (x - x_0)^{-n} \tag{1}$$

(where u^2 stands for two thirds of the turbulent kinetic energy and x is the streamwise distance along the tunnel, x_0 being a virtual origin) differs for different inflow conditions as claimed by George (1992), and if so, how variable can it be.

Lavoie et al. (2007) tried four different conventional passive grids (with square or with round bars with/without a small helical wire) and two different test sections (one with and one without a secondary contraction to improve isotropy). They did not find any significant effect of inflow conditions on the decay exponent n other than that of anisotropy which does, itself, depend on inflow conditions and persists far downstream.

Krogstad and Davidson (2011) carried out a similar wind tunnel study but with two multiscale grids and one conventional grid. Their grids were all monoplanar and their two multiscale grids were chosen from one of the three design families of multiscale grids introduced by Hurst and Vassilicos (2007), specifically the family of fractal cross grids. These grids are very different in design from the low-blockage space-filling fractal square grids which have been used in the vast majority of subsequent works on multiscale/fractal-generated turbulence and which revealed the possibility of a decaying turbulence without the expected high Reynolds number dissipation scaling $A \equiv \varepsilon\ell/u^3 \approx Constant$ (see equation 2) but instead $A \sim Re_\lambda^{-1}$ (read introduction of Valente and Vassilicos (2011) and references therein where, among much else, the consequence of $A \sim Re_\lambda^{-1}$ on fast turbulence decay is also explained). Perhaps the reason why the multiscale/fractal cross grid type of design has mostly been neglected (except in studies where they were used to enhance the Reynolds number, see Kinzel, Wolf, Holzner, Lüthi, Tropea, and Kinzelbach (2010); Geipel, Henry Goh, and Lindstedt (2010)) is that Hurst and Vassilicos (2007) did not make any strong or unexpected claim about the dependence of u^2 on $x - x_0$ in decaying turbulence generated by them. Their conclusion on these grids was just a double negative: "the turbulence decay observed is not in disagreement with power-law fits and the principle of large eddies".

Sketches of the multiscale cross grids used by Krogstad and Davidson (2011) can be seen in their figure 1 and are described in their section 2 where they are labeled *msg1* and *msg2*. We do not need to repeat the description here except to say that each multiscale cross grid has three different mesh sizes, the smallest one being $M_3 = 15mm$ for *msg1* and $M_3 = 21mm$ for *msg2*. Krogstad and Davidson (2011) were careful to design their two multiscale cross grids and one conventional grid in such a way that the longitudinal integral length-scale of the turbulence at a 2m distance from the grid location is the same $\ell_0 \approx 23.65mm \pm 0.25mm$ for all three grids. The ratio between ℓ_0 and the distance between the tunnel walls is smaller than $1/75$.

A description of the wind tunnel used by Krogstad and Davidson (2011) can be found in Krogstad and Davidson (2010, 2011). The grids were placed in the tunnel contraction, specifically 1.2m upstream from the start of their test section, and their turbulence measurements were taken using single and two component hot-wire anemometry from $x \approx 60l_0$ till $x = 400\ell_0$ which means $93M_3 \leq x \leq 629M_3$ for *msg1* and $67M_3 \leq x \leq 446M_3$ for *msg2*. In the case of their conventional grid (refered to as *cg*), $60\ell_0 \leq x \leq 400\ell_0$ corresponds to $40M \leq x \leq 240M$

*p.valente09@imperial.ac.uk; +44 (0) 20759 45050
**j.c.vassilicos@imperial.ac.uk; +44 (0) 207594 5137

where M is the mesh size of the grid.

In the next two sections we apply a careful analysis to the data published by Krogstad and Davidson (2011) which demonstrates that, in the far-region where these authors measure, the multiscale cross grids and the conventional grid produce sig-inicantly different turbulence behaviors, all of which are very clearly different from both Saffman and Loitsyansky turbulence.

2. Decaying homogeneous isotropic turbulence with three different inflow conditions

Krogstad and Davidson (2011) established that their turbulent flows were reasonably homogeneous at x beyond $2m$ in terms of longitudinal profiles of variances, skewnesses and flatnesses of the streamwise fluctuating velocity component. Their centreline mean streamwise flow U remains constant to within less than $\pm 0.1\%$ for all three grids from $x = 2m$ till about $x = 8m$, though it deviates a very little bit for *msg2* beyond $x = 6.5m$. As a result, they chose to design their three grids in such a way that they all generate turbulence with nearly same longitudinal integral length-scale ℓ_0 at $x = 2m$. The positions $x = 80\ell_0$ fall around $1.9m$ for all the grids. (Krogstad and Davidson (2011) in fact recorded, and in a few instances used for their analysis, a few measurements at closer distances to the grid, i.e. x as small as about $41\ell_0$.) The longitudinal length-scale ℓ grows as the turbulence moves downstream, but the ratio between ℓ and the distance between the tunnel walls remains very small, less than about $1/40$ at $8m$ from the grid location.

They also calculated ratios $< u_x^2 > / < u_y^2 >$, $< u_x^2 > / < u_z^2 >$ and $u^2 / < u_x^2 >$ and found small levels of anisotropy "comparable, if not better, than in most other experiments". In particular, $u^2 / < u_x^2 >$ hovers between 0.95 and 1.02 throughout the regions where they recorded their measurements. Hence any anisotropy-related dependence on inflow conditions as in Lavoie et al. (2007) can, most probably, be ruled out.

In figure 1a we plot $< u_x^2 > /U^2$ versus $(x - x_0)/\ell_0$ for all three grids as well as fits of the data by $< u_x^2 > /U^2 \sim (\frac{x-x_0}{\ell_0})^{-n}$. The decay exponents n and virtual origins x_0 in these fits are estimated simultaneously by direct application of a non-linear least-squares regression algorithm ('NLINFIT' routine in MATLAB^{TM}). This fitting method is closely related to the one used by Lavoie et al. (2007) and we apply it to nearly the same range where Krogstad and Davidson (2011) applied their own fitting methods. Specifically, we apply our fit to the range $80\ell_0 < x < 330\ell_0$ which is a range of x from about $1.9m$ to $8m$. This means that, for each grid, we exclude data points obtained by Krogstad and Davidson (2011) at values of x smaller than $80\ell_0$ where according to these authors the turbulence is not sufficiently homogeneous, and we also exclude, exactly like Krogstad and Davidson (2011) do, the data points furthest downstream where noise starts to be significant. (Including data points from $x \approx 1.5m$ (i.e. $60\ell_0$) as in Krogstad and Davidson (2011) makes little difference as the values of n remain the same to within ± 0.01.)

We give the values of n and x_0 thus obtained in table 1 (method I). These values agree fairly well with the various values of n and x_0 obtained by Krogstad and Davidson (2011) by their three different fitting methods for all three grids except for their value of x_0 for *msg1* and their value of n for *msg1* when they use one of their three fitting methods, the regression method (see their table 1). The values of n which they obtain for *msg1* with their other two fitting methods are close to our value of n for *msg1*.

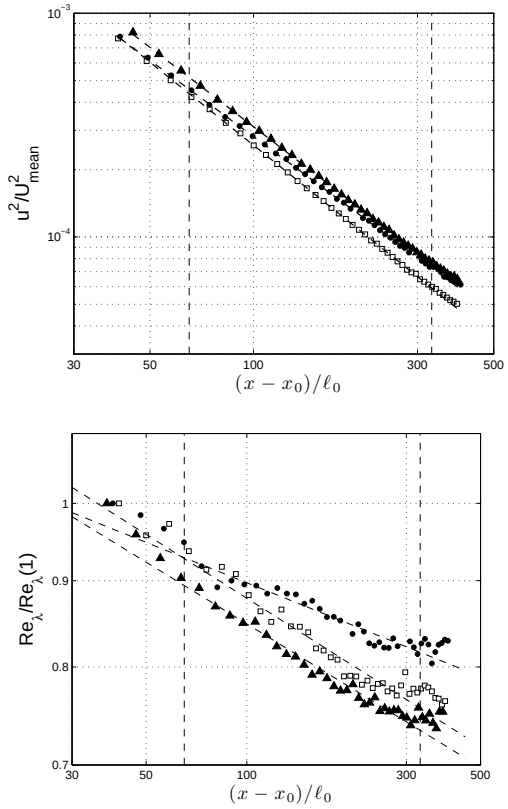

Figure 1: Data and best-fit power laws for: (a) $< u_x^2 > /U^2_{mean}$ versus $(x-x_0)/\ell_0$ (b) $Re_\lambda/Re_{\lambda 1}$ versus $(x - x_0)/\ell_0$. (●) *cg*, (▲) *msg1*, (□) *msg2*. The vertical dashed lines mark the start and end of the admissible data range used in the least-squares fits.

At this point it is helpful to recall some basic theoretical considerations. Homogeneous turbulence in the wind tunnel decays according to $U\frac{d}{dx}\frac{3}{2}u^2 = -\epsilon$ where ϵ is the turbulent kinetic energy dissipation per unit mass. To obtain (1) and the numerical value of n, one needs some more information about u^2 and ϵ. This information usually consists of the following three ingredients when the homogeneous turbulence can also be considered fairly isotropic (see Batchelor and Townsend, 1948; Batchelor, 1953; Rotta, 1972): (i) a finite invariant of the von Kármán-Howarth equation, (ii) the assumption that the decay of large eddies is self-similar and (iii) the empirical assumption that

$$A \equiv \epsilon\ell/u^3 \tag{2}$$

remains constant during decay ($\ell = \ell(x)$ is the longitudinal integral length-scale). This constancy can be thought of as resulting from the assumed independence of A on turbulence intensity and Re_λ.

Vassilicos (2011) proved that there are four different cases of finite invariants of the von Kárman-Howarth equation depending on conditions at infinity. A case where no known finite invariant exists; a case where the Loitsyansky invariant is the only known finite invariant and where self-similar decay of large eddies implies $u^2\ell^5 = const$ during decay; a case where only one known finite invariant exists and where self-similar decay of large eddies implies $u^2\ell^{m+1} = const$ with $2 \leq m < 4$ ($2 \leq m$ ensures that the spectral tensor does not diverge at zero wavenumber as stated in Rotta (1972), in the Appendix of Krogstad and Davidson (2011) and in Vassilicos (2011)); and a case where two finite invariants exist and where, as a consequence, self-similar decay of large-eddies is impossible.

Using the constancies of A and $u^2\ell^{m+1}$, the second and third of these four cases imply

$$n = 2(m+1)/(m+3) \tag{3}$$

where $2 \leq m \leq 4$ and therefore $6/5 \leq n \leq 10/7$. Note that m does not have to be an integer. Also, there is no known way to rule out the fourth case and therefore no known theoretical reason for measured values of n to necessarily lie inside the range $6/5 \leq n \leq 10/7$.

Two out of the three present grids have returned values of n which are below $6/5 = 1.2$ (see table 1 under method I). However, this does not imply that the present turbulence measurements do not fall under the second or third cases identified by Vassilicos (2011). Indeed, as Krogstad and Davidson (2010, 2011) have observed, A varies slowly with x and is therefore not strictly constant. If this is so, then (3) needs to change.

In figure 2 we plot the values of A obtained by Krogstad and Davidson (2011) for their three grids as functions of $(x-x_0)/\ell_0$ where x_0 is taken from table 1 (method I). (Krogstad and Davidson (2011) assumed small-scale isotropy and calculated A from measurements of $<(\frac{\partial u_x}{\partial x})^2>$ using $\epsilon = 15\nu <(\frac{\partial u_x}{\partial x})^2>$ and integrations of measured longitudinal correlation functions to educe ℓ.) To bring out more clearly the differences between grids we in fact plot A/A_1 where A_1 is the value of A obtained at the smallest distance x from each grid. We then follow Krogstad and Davidson (2010) and fit the power law $A \sim (\frac{x-x_0}{\ell_0})^{-p}$ in the range $60\ell_0 < x < 330\ell_0$ of this data. These fits are shown in figure 2 and the values of p are reported in table 1.

If $A = const$ is replaced by $A \sim (x-x_0)^{-p}$ then the implication of $u^2\ell^{m+1} = const$ changes from (3) to

$$n = (1-p)2(m+1)/(m+3) \tag{4}$$

where $2 \leq m \leq 4$. With our estimates of n and p we can now use (4) to derive values of m for each grid. They are given in table 1 (under method I) and, having now taken into account the slight variations of A, they are all between 2 and 4. Similarly, the values of $n' \equiv n/(1-p)$ lie all between $6/5$ and $10/7$ (see table 1 under method I).

These values of m raise the possibility that the three decaying nearly homogeneous and nearly isotropic turbulent flows of Krogstad and Davidson (2011) may be three different instances of the third case identified by Vassilicos (2011) where only one known finite invariant exists and where self-similar decay of large eddies implies $u^2\ell^{m+1} = const$ with $2 \leq m < 4$. The Saffman invariant corresponds to $m = 2$ but none of the grids used by Krogstad and Davidson (2011) returns such a value of m. In figure 3a we plot $< u_x^2 > \ell^{m+1}/(U^2\ell_0^{m+1})$ versus $(x-x_0)/\ell_0$ with the values of m given under method I in table 1 for each one of the three different turbulent flows. This figure should be compared with figure 3c which is a reproduction of figure 10 in Krogstad and Davidson (2011) where they plotted $< u_x^2 > \ell^3/(U^2\ell_0^3)$ versus $(x-x_0)/\ell_0$, except that we have offset the data vertically so as to see more clearly the differences in behavior between each grid. Assuming the turbulence is sufficiently homogeneous and isotropic and equally so for all three flows (as claimed by Krogstad and Davidson, 2011), it is clear that the Saffman prediction is not satisfied in these flows. Instead,

$$u^2\ell^{m+1} = const \tag{5}$$

with $m > 2.5$ for all grids in the range $100\ell_0 \leq x - x_0 \leq 400\ell_0$. Furthermore, different grids give rise to different values of m reaching up to $m \approx 3$ with method I (see table 1).

In fact there is another way to extract values for n and m from the data (method II), and this way gives even better defined invariants and even greater differences between the far downstream turbulence decays originating from the conventional grid and the multiscale cross grids. Method II is based on figure 1b. This figure is a log-log plot of $Re_\lambda/Re_{\lambda 1}$ versus $(x-x_0)/l_0$ where $Re_{\lambda 1}$ is the value of Re_λ at the smallest distance from each grid on this plot and x_0 is the virtual origin obtained from our nonlinear fit of figure 1a. The first inescapable observation is that the streamwise distributions of Re_λ are clearly different for the conventional grid and for the multiscale grids.

The power law form (1) implies $\lambda^2 \sim (x-x_0)$ in decaying homogeneous isotropic turbulence (Batchelor (1953)). If so, it would follow that $Re_\lambda \sim (x-x_0)^{(1-n)/2}$, so that a best fit of the data in figure 1b gives values of n. We apply this power law fit to the very same range $80l_0 < x < 330l_0$ used in method I for our fit of the turbulence intensity data in figure 1a. The values of n thus obtained, the resulting values of m using (4) and the resulting $n' \equiv n/(1-p)$ are given in table 1 under method II. In figure 3b we use these new values of m to plot

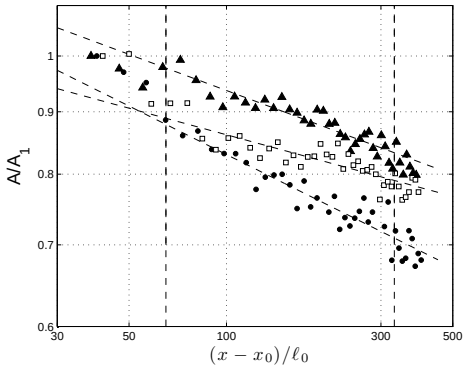

Figure 2: Data and best-fit power laws for A/A_1 versus $(x-x_0)/\ell_0$. (●) *cg*, (▲) *msg1*, (□) *msg2*. The vertical dashed lines mark the start and end of the admissible data range used in the least-squares fits.

Table 1: Estimation of quantities via least squares fit

Grid	p	n	x_0(m)	m	n'	α
Method I						
cg	0.126	1.13	0.23	2.67	1.29	1.90
msg1	0.101	1.18	0.28	2.79	1.31	1.14
msg2	0.072	1.23	0.33	2.94	1.33	0.62
Method II						
cg		1.15		2.85	1.32	1.68
msg1		1.24		3.38	1.37	0.86
msg2		1.25		3.14	1.35	0.57

$< u_x^2 > \ell^{m+1}/(U^2\ell_0^{m+1})$ versus $(x-x_0)/\ell_0$ and find that they yield even better defined invariants (5) than method I (compare with figure 3a) for msg1. The difference between values of m for conventional grids and values of m for multiscale grids is unmistakable and even greater with method II than with method I.

We must conclude that the decay of approximately homogeneous turbulence far from its inflow conditions remains dependent on these inflow conditions. The decay exponent n and the conserved finite invariant $u^2\ell^{m+1}$ both clearly change when the turbulence-generating grid is changed. These inflow conditions may have to do with the geometry of the grids or/and with the inlet Reynolds numbers as the mean speed in the tunnel was $13.5m/s$ when the conventional grid was tested, $14.0m/s$ when *msg1* was tested and $15.5m/s$ when *msg2* was tested.

The mesh size determines the distance between the wakes of the bars and the bar thickness determines the width of these wakes. The Reynolds numbers characterising these wakes (calculated as the mean flow speed multiplied by the bar thickness and divided by the kinematic viscosity of the air) take the values 3.6×10^3 in the case of *cg*; 3×10^3, 1.5×10^3 and 7.5×10^2 in the case of *msg1*; and 3.32×10^3, 1.66×10^3 and 8.3×10^2 in the case of *msg2*. Unlike conventional grids, multiscale grids impose more than one Reynolds number on the flows they generate and a number of different distances from the grid where wakes of different sizes meet. Of course the largest wakes are affected by the wakes generated by the smaller ones. But it is clear that the turbulence undergoes different generation mechanisms extending over different streamwise distances with different grids. It is indeed remarkable that memory of these mechanisms remains in the values of n and m as far downstream as where Krogstad and Davidson (2011) took their measurements.

3. Different far-field low-Re_λ turbulent flows

We obtained figures 3a,b by taking into account the slow streamwise variation of A as suggested by Krogstad and Davidson (2010). This streamwise variation can result from the well-known dependence that the dimensionless dissipation rate A has on Re_λ when Re_λ is below at least 100 (e.g. Burattini, Lavoie, and Antonia, 2005). Indeed, the values of Re_λ characterising the three far-field turbulent flows of Krogstad and Davidson (2011) range between about 90 near $x \approx 60\ell_0$ and 70 at $x \approx 330\ell_0$.

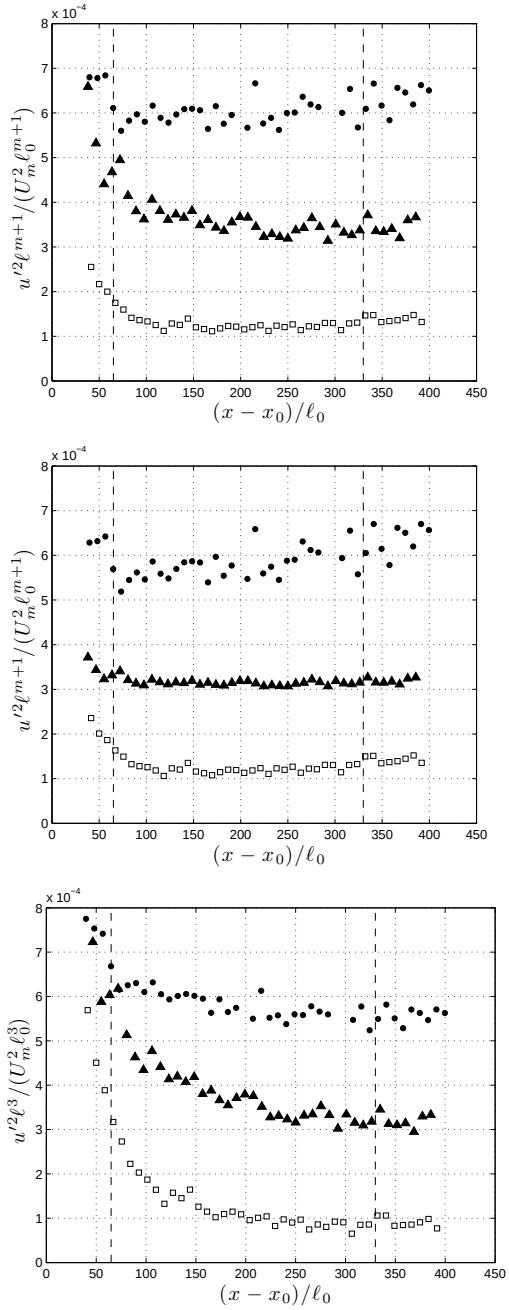

Figure 3: Checks of invariant forms via plots of $u^2\ell^{m+1}$: (a) m from method I, (b) m from method II, (c) $m = 2$ corresponding to Saffman turbulence. (●) *cg*, (▲) *msg1*, (□) *msg2*. For improved readability the *cg*/*msg1*/*msg2* data were vertically offset by (a) $[2.0,\ 1.0,\ 0.0]\times10^{-4}$, (b) $[1.6,\ 2.5,\ 0.0]\times10^{-4}$, (c) $[2.5,\ 0.5,\ -1.5]\times10^{-4}$.The left and right vertical dashed lines mark the start and end of the data range used to obtain the decay exponents n. This is the range not significantly affected by inhomogeneity (to the left) and noise (to the right).

Using $Re_\lambda \sim (x-x_0)^{(1-n)/2}$ and $A \sim (x-x_0)^{-p}$ we obtain

$$A \sim Re_\lambda^\alpha \tag{6}$$

where

$$\alpha = 2p/(n-1). \tag{7}$$

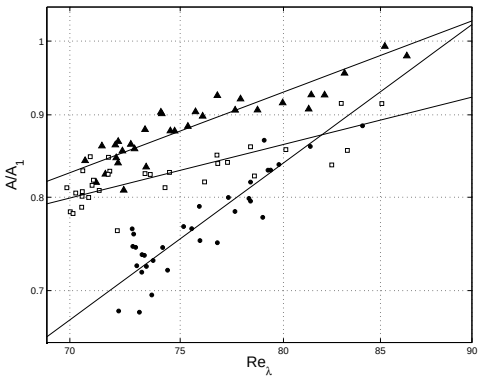

Figure 4: Re_λ dependence of the normalised energy dissipation rate A (note that A here is $3A/2$ in Krogstad and Davidson (2011), for example see their figure 11). (●) *cg*, (▲) *msg1*, (□) *msg2*. The solid lines are plots of $A = const \times Re_\lambda^\alpha$ with α taken from table 1, method II. The axes are logarithmic.

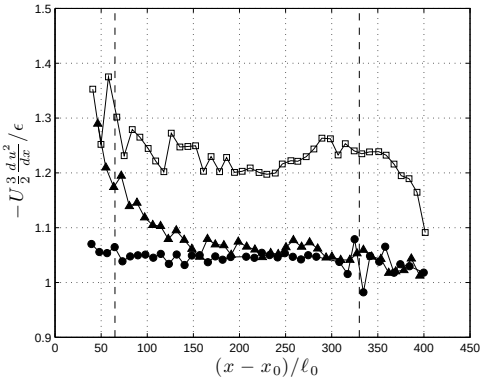

Figure 5: Advection-dissipation balance. (●) *cg*, (▲) *msg1*, (□) *msg2*.

The values of α implied by this formula on the basis of exponents p and n obtained in the previous section are very different for different grids, ranging from $\alpha \approx 1.7$ to $\alpha \approx 0.6$ (using n obtained from method II, see table 1). Figure 4 confirms how dramatically different the dependencies of A on Re_λ are for the multiscale grids and for the conventional grid.

Figure 4 also shows that (6)-(7) give rise to more or less reasonable fits of the data thus lending support to the idea that much of the streamwise variation of A comes from its dependence on Re_λ. Increasing values of the dimensionless dissipation rate A with increasing Re_λ have also been reported in previous works with square bar grids at such relatively low Reynolds numbers, see for example figure 1 in Burattini et al. (2005), table 4 in Comte-Bellot and Corrsin (1971) and table 3 in Gad-El-Hak and Corrsin (1974).

4. Conclusion

According to the published data in Krogstad and Davidson (2011), multiscale cross grids and their equivalent (in terms of ℓ_0) conventional grid can produce very different far-field turbulence with wide variations in the dimensionless dissipation rate's dependence on Re_λ. This would seem to confirm the observation already made by Burattini et al. (2005) on the basis of different Re_λ dependencies of A for different grids, namely that "the geometry of the grid appears to have a persistent influence in the streamwise direction up to $x/M = 80$". In fact the data of Krogstad and Davidson (2011) extend this observation to much further distances downstream and to a wider range of grids.

This data also leads to the conclusion that the decay of the three approximately homogeneous isotropic turbulent flows of Krogstad and Davidson (2011) is characterised by an invariant quantity $u^2\ell^{m+1}$ in the region of the flow $x \geq 80\ell_0$. The exponent m is significantly different from Saffman's $m = 2$ and Loitsyansky's $m = 4$ and ranges between 2.7 and 3.4 for the grids used by Krogstad and Davidson (2011). Their multiscale grids return values of m which are markedly larger than the values of m returned by their conventional grid. The streamwise distributions of Re_λ and A are also very clearly different.

However, in spite of the various homogeneous profiles plotted in Krogstad and Davidson (2011), the *msg2*-generated turbulence is not homogeneous as far downstream as they measure. In figure 5 we plot $-U\frac{d}{dx}\frac{3}{2}u^2/\epsilon$ and find that, for *msg2*, it is larger than 1.2 in the range where $u^2\ell^{m+1}$ is constant with $m \approx 3$. On the other hand, the turbulence generated by *cg* does appear homogeneous in figure 5 in the range where $u^2\ell^{m+1}$ is constant with $m \approx 2.75$. Hence, whereas *msg2* turbulence is not homogeneous enough for the Kárman-Howarth equation to be applicable to it, *cg* turbulence might be. The *msg1* grid which generates a turbulence where $u^2\ell^{m+1}$ is constant with $m \approx 3.4$ where $x - x_0 \geq 90\ell_0$ appears homogeneous in figure 5 only where $x - x_0 \geq 200\ell_0$. This observation suggests that considerations such as those of Vassilicos (2011) which are based on self-similar decay of large eddies and the Kárman-Howarth equation for homogeneous isotropic turbulence in an infinite domain without walls are, at the very least, not sufficient (if at all appropriate) for explaining invariants such as (5), particularly as these invariants might hold over regions which cover both homogeneous and inhomogeneous turbulence. This is an important point which calls for much future research.

We thank Per-Åge Krogstad for providing us with the post-processed data published in Krogstad and Davidson (2011).

Batchelor, G., Townsend, A., 1948. Decay of isotropic turbulence in the initial period. Proceedings of the Royal Society of London. Series A, Mathematical and Physical Sciences 193 (1035), 539–558.

Batchelor, G. K., 1953. The theory of homogeneous turbulence. Cambridge University Press, Cambridge.

Burattini, P., Lavoie, P., Antonia, R., 2005. On the normalized turbulent energy dissipation rate. Physics of Fluids 17, 098103.

Comte-Bellot, G., Corrsin, S., 1971. Simple Eulerian time correlation of full- and narrow-band velocity signals in grid-generated, isotropic turbulence. J. Fluid Mech. 48 (02), 273–337.

Gad-El-Hak, M., Corrsin, S., 1974. Measurements of the nearly isotropic turbulence behind a uniform jet grid. J. Fluid Mech. 62 (01), 115–143.

Geipel, P., Henry Goh, K. H., Lindstedt, R. P., 2010. Fractal-generated turbulence in opposed jet flows. Flow Turbulence Combust. 85 (3–4), 397–419.

George, W. K., 1992. The decay of homogeneous isotropic turbulence. Physics of Fluids A 4 (7), 1492–1509.

Hurst, D. J., Vassilicos, J. C., 2007. Scalings and decay of fractal-generated turbulence. Physics of Fluids 19, 035103.

Kinzel, M., Wolf, M., Holzner, M., Lüthi, B., Tropea, C., Kinzelbach, W., 2010. Simultaneous two-scale 3D-PTV measurements in turbulence under the influence of system rotation. Exp Fluids(to appear).

Krogstad, P. r., Davidson, P. A., 2010. Is grid turbulence Saffman turbulence? J. Fluid Mech. 642, pp 373–394.
Krogstad, P. r., Davidson, P. A., 2011. Freely decaying, homogenous turbulence generated by multi-scale grids. J. Fluid Mech. 680, 417–434.
Lavoie, P., Djenidi, L., Antonia, R., 2007. Effects of initial conditions in decaying turbulence generated by passive grids. J. Fluid Mech. 585, 395–420.
Rotta, J. C., 1972. Turbulente Strömungen: eine Einführung in die Theorie und ihre Anwendung. B.G. Teubner, Stuttgart.
Valente, P. C., Vassilicos, J. C., 2011. The decay of homogeneous turbulence generated by a class of multi-scale grids. J. Fluid Mech.(Available on CJO doi:10.1017/jfm.2011.353).
Vassilicos, J. C., 2011. An infinity of possible invariants for decaying homogeneous turbulence. Physics Letters A 375 (6), 1010 – 1013.